Influence of the Solvent Environment on the Ultrafast Relaxation Pathways of a Sunscreen Molecule Diethylamino Hydroxybenzoyl Hexyl Benzoate

Min-Hsien Kao, Ravi Kumar Venkatraman[1], Mahima Sneha, Matthew Wilton and Andrew J. Orr-Ewing*
School of Chemistry, University of Bristol, Bristol BS8 1TS, UK.

[1] Current address: Department of Inorganic and Physical Chemistry, Indian Institute of Science, Bangalore 560012, India.

* Author for correspondence: a.orr-ewing@bristol.ac.uk

ABSTRACT

The excited-state dynamics of photoexcited diethylamino hydroxybenzoyl hexyl benzoate (DHHB), a UVA absorber widely used in sunscreen formulations, are studied with transient electronic and vibrational absorption spectroscopy methods in four different solvents. In the polar solvents methanol, dimethyl sulfoxide (DMSO) and acetonitrile, strong stimulated emission (SE) is observed at early time delays after photoexcitation at a near-UV wavelength of λ_{ex} = 360 nm, and decays with time constants of 420 fs in methanol and 770 fs in DMSO. The majority (~95%) of photoexcited DHHB returns to the ground state with time constants of 15 ps in methanol and 25 ps in DMSO. In the non-polar solvent cyclohexane, ~98% of DHHB photoexcited at λ_{ex} = 345 nm relaxes to the ground state with a ~10 ps time constant, and the SE is weak. DHHB preferentially adopts an enol form in its ground S_0 state, but excited state absorption (ESA) bands seen in TEAS are assigned to both the S_1-keto and S_1-enol forms, indicating a role for ultrafast intramolecular excited state hydrogen transfer (ESHT). This ESHT is inhibited by polar solvents. The two S_1 tautomers decay with similar time scales to the observed recovery of ground state population. For molecules that avoid ESHT, torsion around a central C-C bond minimizes the S_1-enol energy, quenches the SE, and is proposed to lead to a conical intersection with the S_0 state that mediates the ground state recovery. A competing trans-enol isomeric photoproduct is observed as a minor competitor to parent recovery in polar solvents. Evidence is presented for triplet (T_1) enol production in polar solvents, and for T_1 quenching by octocrylene, a common UVB absorber sunscreen additive. The T_1 keto form is observed in cyclohexane solution.

I. Introduction

UV light from the sun is commonly divided into three wavelength regions: UVA (400-320 nm), UVB (320-280 nm) and UVC (280-100 nm), of which UVA accounts for more than 90% of UV radiation reaching the surface of the Earth.[1] This UVA can penetrate human skin to the dermis layer.[2] Although DNA mainly absorbs UVB radiation, UVA absorption encourages formation of reactive oxygen species that can cause DNA damage and increase the occurrence of skin cancers.[3-6] The application of UVA absorbers to the skin inhibits the generation of these reactive oxygen species and reduces oxidative stress in cultured human dermal fibroblasts exposed to UVA.[3, 7]

Diethylamino hydroxybenzoyl hexyl benzoate (DHHB), with the structure shown in Figure 1, is a UVA absorber widely approved for use in sunscreens in Japan, Europe, Australia and South Africa with commercial name Uvinul A .[8, 9] Previous studies of DHHB focused on its photostability in formulations with other sunscreen molecules such as tert-butyl-methoxydibenzoylmethane and avobenzone.[10-12] DHHB has a similar core structure to oxybenzone (see Figure 1c), which is an efficient UVB absorber but toxic to coral and now a banned ingredient of sunscreen products in Hawaii.[13, 14] Prior ultrafast spectroscopy studies have established that the relaxation mechanism of photoexcited oxybenzone is via enol → keto tautomerization.[15] After UV excitation of the ground-state enol form to the S_2 state, oxybenzone undergoes excited state hydrogen transfer (ESHT) to reach the S_1-keto form on a time scale estimated to be ~100 fs.[15, 16] Following ESHT, the keto form of oxybenzone experiences central C-C bond torsion with a time constant of around 400 fs, and the twisted keto S_1 state molecules access a conical intersection (CI) which provides an efficient relaxation pathway to the ground electronic state. In oxybenzone, this ground-state recovery takes ~8 ps and there is a small yield of an isomer, the trans-keto form, which relaxes back more slowly to the lowest-energy form.[15-17] In addition, after photoexcitation to the singlet excited state, a minor pathway involving formation of the phenoxy radical of oxybenzone by homolytic H-O bond cleavage was reported at longer timescales.[18]

DHHB differs from oxybenzone by the presence of an auxochrome amino group meta to the -OH group on one phenyl ring. The amino group shifts the main $\pi^*\leftarrow\pi$ absorption band by 15 nm to longer wavelength than for oxybenzone in cyclohexane solution. This $\pi^*\leftarrow\pi$ absorption band of DHHB is sensitive to the solvent polarity, undergoing a bathochromic shift as can be seen in Figure S3 of Supporting Information. The presence of an additional auxochrome, the ester group of DHHB connected to the other aromatic ring, facilitates charge separation in the first excited singlet state, and thereby modifies the photochemistry in ways that are explored here. A simpler molecular analogue of both DHHB and oxybenzone, 2-hydroxy-benzophenone, has been reported to have different photophysical properties in ethanol and hexane, and a long-lived absorption signal in ethanol was assigned to triplet state photoproducts.[19] The photochemical

properties of DHHB have also been shown to depend on the solvent. In ethanol, DHHB is phosphorescent at 77 K, but in non-polar solvents it does not phosphoresce, suggesting that the intramolecular hydrogen bond between the OH and carbonyl groups, which is expected to be sensitive to the solvent environment, plays an important role in the relaxation of photoexcited DHHB.[20]

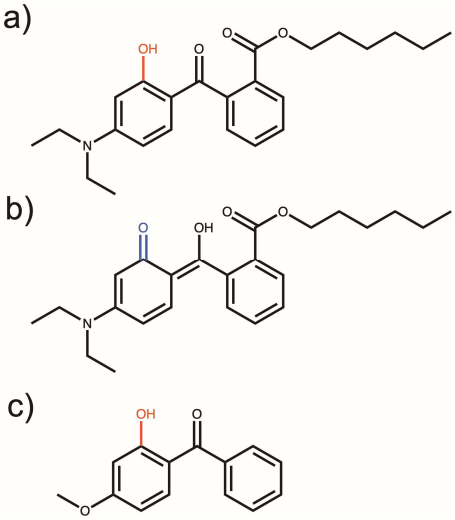

Figure 1. Molecular structures of: (a) DHHB in its enol form; (b) DHHB in its keto form; (c) oxybenzone.

Formation of triplet species is undesirable for sunscreen molecule since they can be quenched by O_2 to form singlet oxygen which is a reactive oxygen species.[21, 22] In addition, triplet-triplet energy transfer between UVA and UVB absorbers has been reported to reduce the efficiency of sunscreen products.[23, 24] DHHB has a similar triplet state energy to both octocrylene and octyl methoxycinnamate sunscreen additives, so triplet DHHB may be quenched by these compounds,[20, 25] but with potential consequences for the effectiveness of these UVB filters.

The ultrafast transient electronic and vibrational absorption spectroscopy (TEAS and TVAS) studies reported here compare the photochemical properties of DHHB and its primary relaxation pathways in four solvents, cyclohexane (CYCH), methanol (MeOH), acetonitrile (ACN), and dimethyl sulfoxide (DMSO). Competition is identified in the UV-excited S_1 state between torsional motion in the enol form towards an $S_1 - S_0$ conical intersection, ESHT from the enol to keto forms, and intersystem crossing to the triplet manifold of states, with solvent-dependent outcomes. Relaxation mechanisms of photoexcited DHHB are proposed, the associated time constants are reported, and the outcomes are contrasted with the relaxation pathway for the structurally similar oxybenzone. Evidence is presented for a minor photochemical role for triplet-state DHHB.

II. Experimental and Computational Methods

Acetonitrile (Fisher, HPLC grade, ≥ 99.9%), cyclohexane (Acros, for spectroscopy, > 99%), dimethyl sulfoxide (Merck, Uvasol for spectroscopy) and methanol (Sigma-Aldrich, HPLC grade, ≥ 99.9%) were used to prepare 25 mM stock solutions of diethylamino hydroxybenzoyl hexyl benzoate (BASF Uvinul A Plus, 99.7%). Octocrylene (Supelco, Pharmaceutical Secondary Standard) or trans-β-methyl styrene (Sigma-Aldrich, 99%) were added to some of the prepared DHHB solution samples to test triplet-triplet energy transfer pathways. All the chemicals were used without further purification.

Samples used for steady state and transient absorption spectroscopy studies were prepared from the stock DHHB solutions, by dilution if required. Absorption spectroscopy measurements were performed using a stainless-steel Harrick cell fitted with two 1.5-mm thick CaF_2 windows separated by 100-μm polytetrafluoroethylene (PTFE) spacers. Steady state UV-visible spectra of 2.5 mM solutions were measured by a GENESYS 10S UV-Vis Spectrophotometer (Thermo Scientific). The IR absorption spectra of 25 mM DHHB solutions were obtained using a Spectrum Two FTIR Spectrometer (PerkinElmer). Fluorescence emission spectroscopy of 25 μM DHHB solutions instead used a 1 cm-pathlength quartz cuvette placed into a fluorimeter (PerkinElmer LS 45) with slits set at 10 nm wavelength resolution.

The ultrafast laser system and associated spectrometers and optical paths used for TEAS and TVAS measurements have been described in detail in previous publications.[26, 27] 2.5 mM DHHB solutions were continuously circulated from a reservoir to a stainless-steel Harrick cell fitted with CaF_2 windows separated by 100 μm. The reservoir and cell were connected by PTFE tubing, and circulation was maintained by a peristaltic pump. TEAS and TVAS data acquisition used custom-written Labview software, and the spectral data were processed and decomposed using the KOALA program.[28] The near-UV excitation wavelength was set at λ_{ex} = 360 nm for DHHB solutions in polar solvents, and at λ_{ex} = 345 nm for solutions in CYCH, corresponding to wavelengths close to the absorption maxima of the long-wavelength bands of DHHB in these solvents. The excitation was increased to 375 nm for studies of triplet quenching with octocrylene to minimize overlap with the red edge of the octocrylene absorption band. The wavelength region covered by the white-light continuum TEAS probe beam was from 330 nm to 700 nm, and the mid-IR TVAS probe spanned 1550 - 1800 cm^{-1} to monitor the carbonyl stretching region. Instrument responses were ~120 fs for TEAS and 150 fs for TVAS. The possible degradation of the DHHB sample, and hence accumulation of photoproducts during measurements, was monitored by recording the UV-visible absorption spectrum of the solution before and after the time-resolved experiments. Any loss of DHHB absorption was always observed to be less than 2%.

All the calculations of vibrational frequencies, excited state energies and structures reported here were performed using the Gaussian 09 package.[29] Density functional theory (DFT) calculations of optimized geometries and IR spectra for the ground state species used the B3LYP functional with a 6-31G** basis set and the conductor-like polarizable continuum model (CPCM) to treat the solvent environment.[30-36] Simulated UV-Vis spectra, as well as optimized geometries and IR absorption band frequencies for the excited electronic states were calculated with time-dependent density functional theory (TDDFT) with the B3LYP functional at the 6-31G** CPCM level.[37]

III. Results and Discussion

III.I DHHB Structures in the Ground and Excited Electronic States

Figure 1 shows the two tautomeric forms of DHHB. The enol form is significantly more stable than the keto form in the ground (S_0) electronic state, and our calculations suggest a barrierless process to go from the keto to the enol form (Figure S1 of Supporting Information). Therefore, for all the experiments conducted here, excitation is assumed to be from DHHB (S_0) in its enol form. The optimized S_0 structure from our calculations is shown in Figure S2 of Supporting Information, and is close to planar in the region of the central carbonyl group and the phenolic ring, but with an out-of-plane twist (by ~47°) of the second aromatic ring to reduce steric repulsions. The experimental and computational UV-Vis absorption spectra of DHHB are shown in Figure S3 of Supporting Information. UV excitation of DHHB near the maximum of the first absorption band, with λ_{ex} = 360 nm (or 345 nm in CYCH) corresponds to an $S_0 \rightarrow S_1$ transition, and our transient spectroscopy studies therefore do not involve dynamics in higher lying electronically excited states. This first electronic transition consists of a HOMO to LUMO $\pi \rightarrow \pi^*$ electronic excitation, and the shift to longer wavelength in more polar solvents is typical for this type of transition.[38-40]

Vertical excitation initially populates the S_1 state in an enol geometry (henceforth S_1-enol) in the Franck-Condon (FC) region with coplanar central carbonyl and hydroxyl groups. As Figure S2 shows, the optimized geometry of the S_1 enol is computed to have a twisted structure in which rotation about a central C-C bond brings the two phenyl rings to an almost perpendicular orientation. In this structure, the C(OH)-C-C=O dihedral angle is 67°. The excited MO in the optimized S_1 enol geometry is located mostly on the phenyl ring with the pendent ester group, corresponding to charge transfer (CT) character for this region of the S_1-enol PES (Figure S2). This CT-character in the twisted S_1 enol will be stabilized by polar solvents. In the vertical excitation region (for the heavy atoms), the S_1-keto form of DHHB, resulting from excited state hydrogen transfer (ESHT), is computed to lie lower in energy in methanol than the corresponding S_1-enol structure, and the optimized geometry is shown in Figure S2. The dynamics from the FC region of the

initially excited S_1-enol molecules are therefore expected to be either ESHT to the keto form or torsion about a central C-C bond to reach the lower energy region of the twisted S_1-enol form. This model for evolution of the excited state structures is summarized schematically in Figure 2 and forms the basis for the interpretation of transient absorption spectroscopy data reported here. These measurements provide evidence for competing ESHT and torsional dynamical pathways in the S_1 excited state, quantify time constants for the pathways, and show how the competition is affected by different types of interactions with the surrounding solvent.

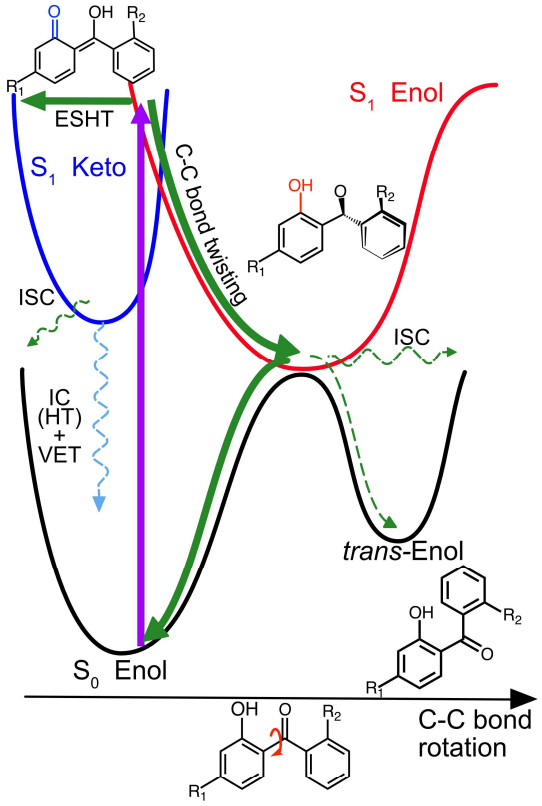

Figure 2. Illustrative PESs along the C-C bond rotation coordinate and significant photochemical pathways of DHHB. After vertical excitation from the S_0-enol state to the S_1-enol state, there is competition between ESHT to the S_1-keto form and relaxation on the S_1 PES to the lower energy twisted S_1-enol structure. The majority of photoexcited molecules relax to the ground state, and only a small fraction undergoes intersystem crossing (ISC) to populate triplet states, or forms an isomeric photoproduct denoted as *trans*-enol in the S_0 state. The S_1-keto tautomer may relax to the ground state via direct internal conversion (IC) and vibrational energy transfer (VET), or via reverse ESHT to the S_1-enol form.

III.II Transient Electronic Absorption Spectroscopy of DHHB

III.II.I Solvent-Dependent Photodynamics. Figure 3 shows TEA spectra of DHHB in different solvents. In spectra obtained at delays of up to a few picoseconds, strong negative signals at wavelengths around 500 nm for solutions in polar solvents are assigned as stimulated emissions (SE), but the corresponding SE for DHHB in CYCH is weak. These observations are consistent with the steady state fluorescence spectra

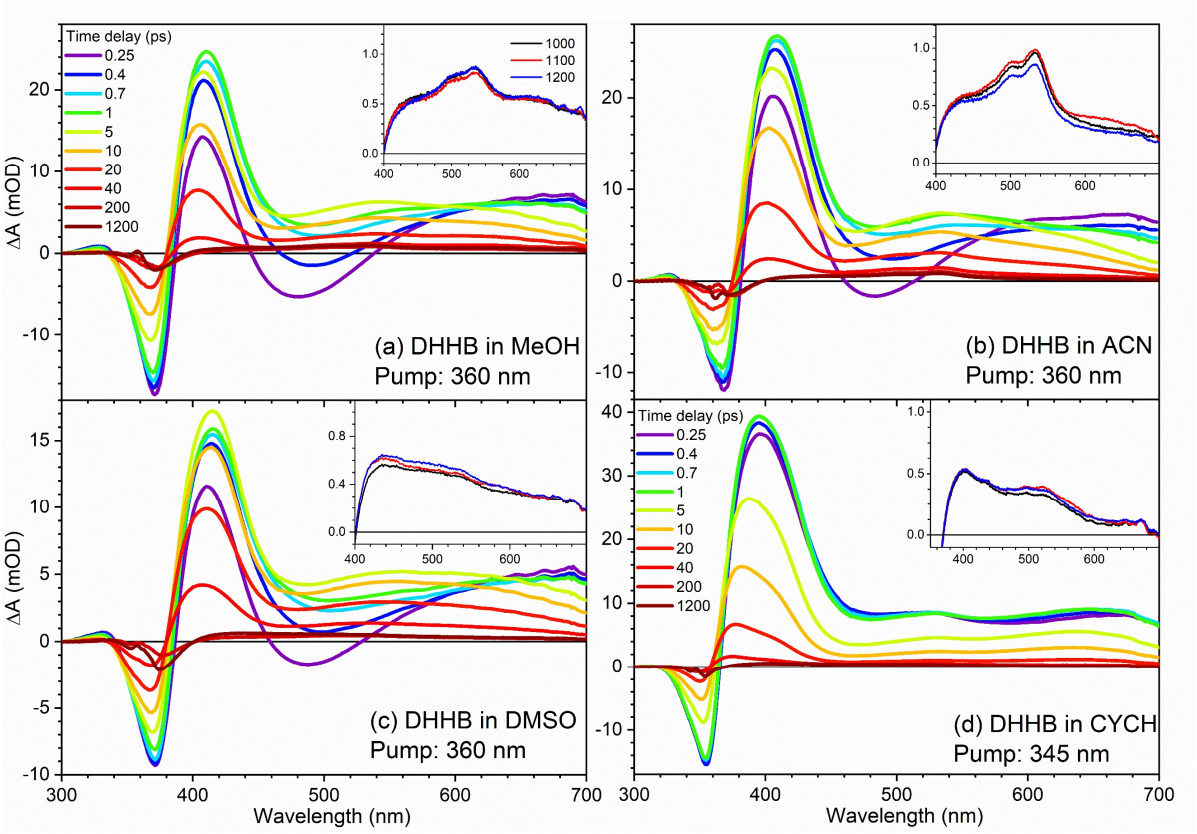

Figure 3. Transient electronic absorption spectra of DHHB in (a) methanol, (b) acetonitrile, (c) dimethyl sulfoxide and (d) cyclohexane. A colour key for the time delays corresponding to different spectra is shown in panel (a). The late time spectra are shown on an expanded scale as insets in each panel.

shown in Figure S4; these spectra show no discernable fluorescence from DHHB in CYCH under conditions in which weak fluorescence emission is detected from solutions in methanol, acetonitrile and, most prominently, DMSO. The late-time TEA spectra, the long-wavelength regions of which are shown as insets in each panel, indicate further differences between DHHB photochemistry in the non-polar solvent and polar solvents, and will be discussed later. SE at sub-ps to few-ps delay times is likely to derive from the photoexcited DHHB in the S_1-state FC region, and its decay is a measure of the onset of excited state dynamics. These dynamics might involve either S_1 keto formation by ESHT or structural relaxation to the twisted S_1 enol (Figures 2 and S2) with loss of excess vibrational energy to the solvent. Both pathways

change the geometry of the excited-state DHHB and its electronic character, and hence are expected to quench the SE, but the surrounding solvent environment affects their time scales and changes the balance of competition.

The intensity of the observed SE bands appears to relate to the hydrogen bonding ability of the chosen solvent. The strongest DHHB SE feature is seen in solution in MeOH, which can act as both a hydrogen bond donor and acceptor, whereas ACN and DMSO, in which the SE bands are somewhat less pronounced, are poorer hydrogen bond acceptors.[41] In CYCH, which does not form conventional hydrogen bonds, signatures of SE are barely evident. The prominence of the SE feature is therefore proposed to be evidence for disruption by H-bonding solvents of the ESHT mechanism for S_1 enol to S_1 keto conversion in the initially excited FC region. In CYCH solution, the solvent does not interfere with this pathway and we propose that the SE from the photoexcited S_1-enol form (as well as steady state fluorescence) is rapidly quenched by ESHT. Figure S5 shows relaxed scans of the computed potential energy changes from the optimized S_1-keto to the FC region S_1-enol form, performed using CPCM treatments of MeOH and CYCH. Although the CPCM method does not treat explicit solvent-solute interactions, the calculations indicate that ESHT is a barrierless process in CYCH, whereas in MeOH there is a barrier estimated to be ~10 kJ mol^{-1}. Therefore, the rate of ESHT is expected to be dependent on the polarity of the solvent environment.

The excited state absorption (ESA) band peaking near 410 nm, and extending to longer wavelength, rises at early times as the partially overlapping SE feature decays in amplitude. Its maximum intensity is greater in CYCH than in MeOH, ACN and DMSO solutions, and it closely resembles a prominent ESA band observed in TEAS studies of oxybenzone that was assigned to an S_1-keto form.[15] On the basis of this evidence, and electronic structure calculations of the absorptions from the S_1 enol and keto forms (see Figure S6), the 410-nm ESA band seen for DHHB solutions is assigned to the S_1-keto product of ESHT. A broader ESA band extending to longer wavelength is instead attributed to the S_1-enol form. Hence, ESHT is not the only observed pathway after photoexcitation, and both S_1 keto and enol forms contribute to the TEA spectra.

III.II.II Spectral Decomposition and Kinetic Analysis of TEAS data. The decomposition of DHHB TEA spectra obtained in the polar solvents into constituent absorption bands is achieved using five spectral basis functions. One of these functions models the time-evolution of the SE, and another one accounts for the changing intensity of the 410-nm ESA band of the S_1-keto DHHB. The third basis function describes changes to the ground-state bleach (GSB) feature evident at wavelengths around 360 nm. The fourth accounts for long wavelength spectral features, and it thus includes the long-wavelength ESA feature assigned to the S_1 enol (see above) at early time delays. Finally, the fifth basis function is used fit the late

time spectra and grows with a fixed time constant chosen to be close to the S_1-enol lifetime. It is interpreted as representing ESA from triplet states (see below). For the decomposition of DHHB TEA spectra obtained in CYCH, a SE basis function was not required. None of the spectra shown in Figure 3 show any evidence of SE from the S_1 keto state in the probe wavelength window. Any such SE bands would be expected to decay on the same timescale as the loss of the S_1 keto ESA. Further details of the basis functions used are provided in the Supporting Information, and examples of the decomposition of TEA spectra in methanol and CYCH are illustrated in Figures S7 and S8.

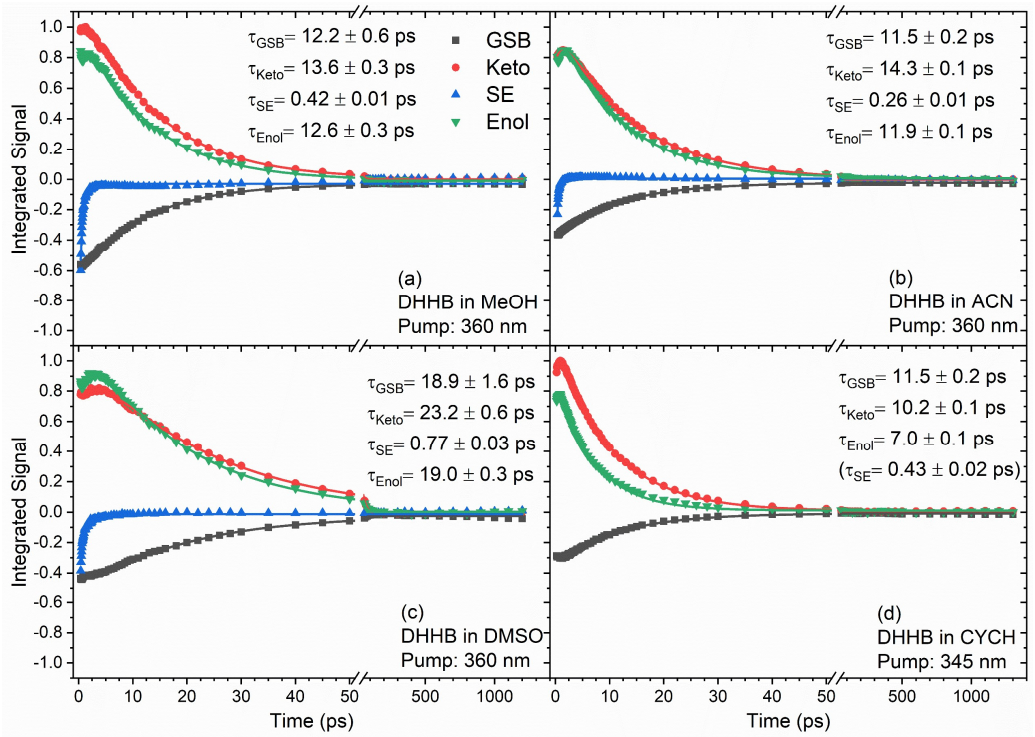

Figure 4. Time dependence of the wavelength-integrated intensities of GSB (black), ESA of keto (red), SE (blue) and ESA of enol (green) features for UV-photoexcited DHHB in: (a) methanol, (b) acetonitrile, (c) dimethyl sulfoxide and (d) cyclohexane. The time constants obtained from exponential fits are shown in each panel. The integrated intensities are derived from spectral decomposition of TEA spectra shown in Figure 3 using methods described in the main text.

Figure 4 shows how the wavelength-integrated intensities of the basis functions fitted to the evolving TEA spectra change with time. The first three data points (Δt= 0.25, 0.3, 0.35 ps) in polar solvents showed unreasonably sharp decay or growth, which is attributed to fitting artefacts from the overlap of the basis functions. These first three time points were therefore excluded in subsequent kinetic fitting. The kinetics

of the GSB, S_1-keto and S_1-enol components were globally fitted to extract exponential time constants reported in Figure 4 and Table 1. The kinetics of SE decay are mono-exponential in MeOH, DMSO and ACN. Although an SE basis function was not used to fit TEA spectra in CYCH, an early time rise in the intensities of the S_1 ESA features evident in Figure 4(d) is suspected to derive from decay of a weak, overlapping SE contribution. Therefore, the time constant for DHHB S_1 SE decay in CYCH is estimated from global fitting of a shared time constant to the early time changes in S_1-keto, S_1-enol and GSB band intensities.

From this kinetic analysis, the time constants obtained for DHHB S_1 SE decay (τ_{SE}) range from ≤400 fs (in MeOH and ACN) to almost 800 fs (in DMSO), and the time constants for the ESA decays (τ_{Keto} and τ_{Enol}, corresponding to the S_1 keto and enol contributions) are in the range of 7 to 23 ps, also with dependence on the solvent. The time constants extracted from TEAS analysis are summarized in Table 1.

Table 1. Relaxation Time Constants Obtained from TEAS and TVAS in Four Solvents.[a]

	MeOH	ACN	DMSO	CYCH
τ_{GSB} (from TEAS)	12.2 ± 0.6 ps	11.5 ± 0.2 ps	18.9 ± 1.6 ps	11.5 ± 0.2 ps
τ_{Keto}	13.6 ± 0.3 ps	14.3 ± 0.1 ps	23.2 ± 0.6 ps	10.2 ± 0.1 ps
τ_{SE}	0.42 ± 0.01 ps	0.26 ± 0.01 ps	0.77 ± 0.03 ps	0.43 ± 0.02 ps
τ_{Enol}	12.6 ± 0.3 ps	11.9 ± 0.1 ps	19.0 ± 0.3 ps	7.0 ± 0.1 ps
τ_{GSB} (from TVAS)	14.7 ± 0.4 ps	14.8 ± 0.3 ps	25.0 ± 0.8 ps	12.5 ± 0.2 ps

[a] τ_{SE}, τ_{Keto}, τ_{Enol} and τ_{GSB} are time constants for SE decay, ESA of the S_1 keto decay, ESA of the S_1 enol decay, and S_0 enol GSB recovery respectively. In CYCH, SE is not clearly observed, but an early time rise in the ESA intensity is attributed to loss of overlapping SE signal.

In prior oxybenzone studies, a time constant of ~400 fs was attributed to torsional motion in the S_1-keto form as it relaxed to its minimum energy twisted geometry.[15-17] However, in the case of DHHB our calculations show a preferred S_1-keto structure that maintains the near planarity of the OH and carbonyl groups, with the relaxed S_1 enol instead showing the corresponding twisted structure (Figure S2). The τ_{SE} = 300 fs – 800 fs time constants reported here are therefore assigned to the torsional motion of the S_1-enol tautomer, as is illustrated in Figure 2, while it undergoes relaxation to the S_1-enol minimum energy structure. Any excess energy in the initially photoexcited S_1 DHHB will evolve into vibrational excitation and then be dissipated to the solvent bath. The time constants for decay of SE features apparently relate to solvent viscosity: in the more viscous DMSO, τ_{SE} = 770 fs is consistent with greater resistance from the solvent to the incipient C-C bond twisting.

The time constant for excited-state hydrogen atom transfer (τ_{ESHT}) is expected to be 100 - 200 fs on the basis of observations in similar compounds.[42, 43] For example, ESHT dynamics in other common sunscreen molecules like homosalate, oxybenzone and methyl salicylate are reported to occur within 200 fs.[16, 44, 45] ESHT in DHHB on such timescales is not directly observed in our measurements, but is compatible with quenching of most of the SE from DHHB (S_1 enol) in CYCH within our ~150 fs TEAS instrument response.

The ESHT is suggested to be inhibited in polar solvents because of disruption of the intramolecular hydrogen bond in DHHB. Our calculated PESs along the ESHT coordinate (Figure S5), obtained using the CPCM solvation model, predict an ESHT barrier in methanol, but no such barrier in CYCH. In the latter solvent, the majority of photoexcited DHHB molecules therefore undergo ESHT, converting to the S_1-keto form within 200 fs. A minor fraction of photoexcited DHHB remains in the S_1-enol form to undergo structural relaxation via C-C bond torsion In contrast, in the polar solvents, ESHT dynamics are proposed to occur more slowly (i.e. >200 fs). The more prominent SE from the S_1-enol form of DHHB observed in spectra in Figures 3(a)-(c) is consistent with competition between this slower ESHT and the aforementioned torsional dynamics about the C-C bond that drive the S_1 enol towards its lowest energy. As is noted above, evidence for this competition comes from the ESA bands assigned to both S_1-keto and S_1-enol tautomers. As the S_1-enol form twists from its initially excited form in the Franck-Condon region, it drops in energy and the energy of the corresponding S_1-keto form increases (see Figure 2). Hence the torsional motion rapidly switches off the ESHT pathway, leaving populations of the S_1 enol (in a twisted geometry) and the S_1 keto to evolve separately thereafter.

The later time TEA spectra of DHHB in DMSO shown in Figure 3(c) differ from those obtained in MeOH and ACN, and they are instead more similar to those obtained for solutions in CYCH. The weak, long-wavelength features observed are discussed below. These similarities are consistent with slower C-C bond torsion in the more viscous DMSO providing a more extended window of opportunity for ESHT than for DHHB solutions in MeOH and ACN.

The τ_{Enol} = 7 – 20 ps time constants for decay of S_1-enol ESA, with values depending on the solvent, are attributed to electronic relaxation of the excited DHHB from its S_1-enol to the S_0 electronic ground state. The relaxation pathway is likely to involve a conical intersection between the S_1 and S_0 states with a twisted central C-C bond (Figure 2), and the time constants of GSB recovery, τ_{GSB}, in TEAS are consistent with the τ_{Enol} values (Table 1), except perhaps in CYCH where S_1-keto relaxation is argued to be more significant. The τ_{Keto}= 10 - 23 ps time constants for S_1 keto decay are consistently slightly longer than the corresponding τ_{Enol} values in the same solvent. The differences may result from an alternative decay pathway mediated by a separate CI in the keto form, or delayed reverse ESHT to repopulate the S_1-enol form before $S_1 \rightarrow S_0$ relaxation.

III.III Transient Vibrational Absorption Spectroscopy of DHHB

III.III.I Ground-State DHHB Recovery. The electronically non-adiabatic dynamics of $S_1 \rightarrow S_0$ relaxation were studied further with the aid of TVA spectra, examples of which are shown in Figure 5 for DHHB in various solvents. On the basis of bands observed in steady state FTIR spectra (Figure S9), the negative-going transient absorption bands around 1633 cm^{-1} and 1725 cm^{-1} are assigned as ground state bleaches arising from photoexcitation of DHHB (S_0). The GSB in CYCH recovers nearly to baseline within the limiting 1200 ps time delay of our measurements, indicating that most of the photoexcited DHHB relaxes back to the ground state. In contrast, noticeable GSB features remain at the later time delays in all the polar solvents. In addition to these remaining GSB features, there are positive bands in the TVA spectra round 1600 cm^{-1} at these later times for DHHB dissolved in the polar solvents.

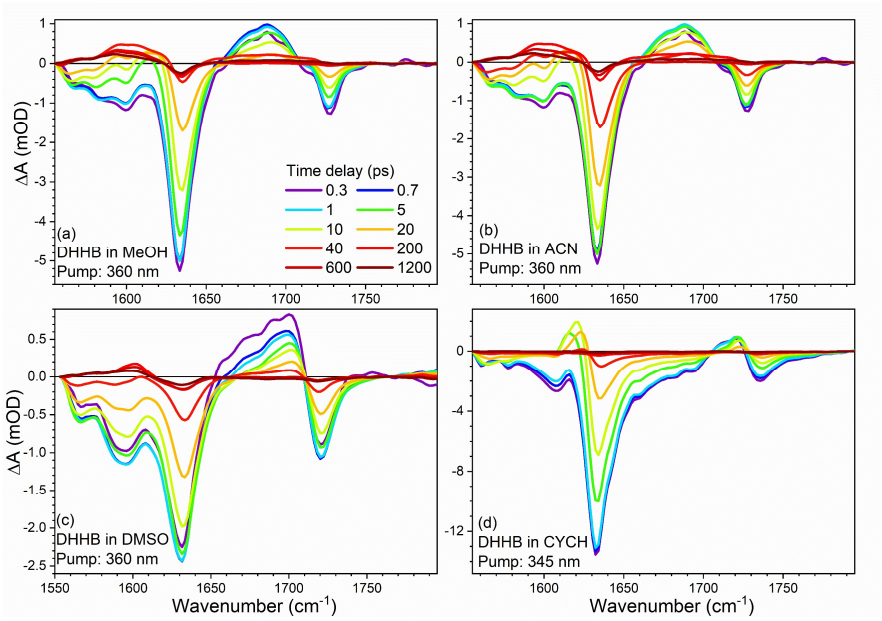

Figure 5. TVA spectra of DHHB in: (a) methanol; (b) acetonitrile; (c) dimethyl sulfoxide; and (d) cyclohexane. The colour key in panel (a) shows the time delays corresponding to different spectra. The near-UV excitation (pump) wavelengths used are specified in the panels.

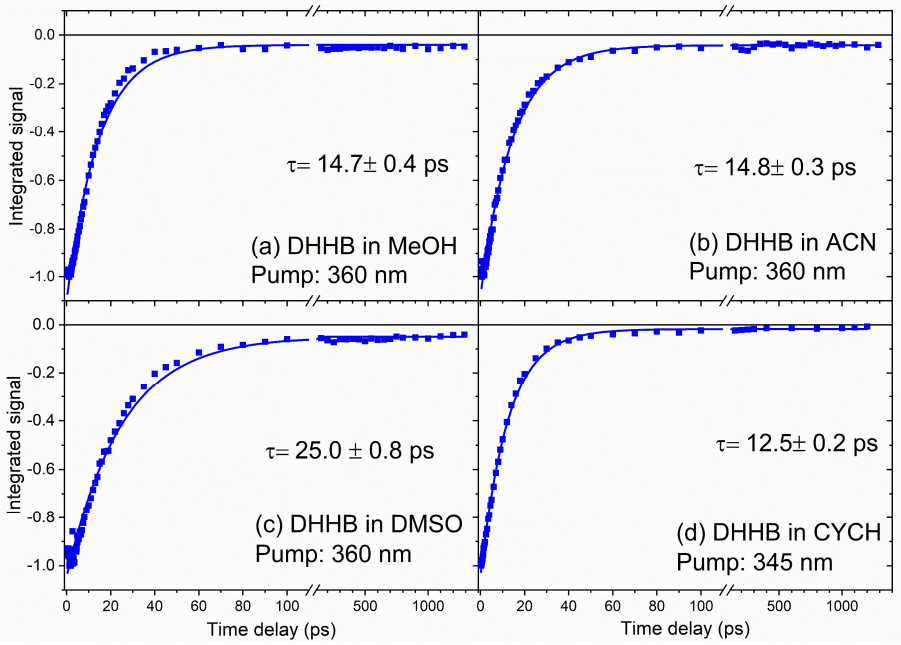

Figure 6. Kinetics of DHHB ground-state bleach recovery for the band with centre at ~1633 cm^{-1} in: (a) methanol, (b) acetonitrile, (c) dimethyl sulfoxide and (d) cyclohexane. Single exponential time constants from fits shown as solid lines are reported in each panel.

The kinetics of the GSB recoveries obtained by integrating the intensities of the features centred at ~1633 cm^{-1} are shown in Figure 6, together with single-exponential fits. Values of the resulting time constants (τ_{GSB} from TVAS) are reported in Table 1; these values are in the 12 - 25 ps range, and are slightly longer than those extracted from the analysis of TEA spectra. Hence, they are assigned to $S_1 \rightarrow S_0$ relaxation via one or more conical intersections. The GSB recovery in TVAS is obtained from repopulation of S_0 molecules in their lowest vibrational level, so the recovery time constants will be affected by vibrational cooling in the S_0 state, as well as reflecting the kinetics of $S_1 \rightarrow S_0$ electronic relaxation which are derived from the TEAS analysis.

III.III.II Minor Photoproduct Formation. Our calculations show the optimized S_1-enol structure is twisted, and we propose S_1 to S_0 internal conversion via a conical intersection in this region. Hence, as the molecules relax through the CI to repopulate the S_0 state, the C-C bond could keep twisting to form a *trans*-enol S_0 isomer instead of reverting to the minimum energy S_0 geometry. Figure S10 compares calculated IR spectra of the *trans*-enol and *trans*-keto forms of DHHB (S_0) with the late time TVA spectra of DHHB in methanol. The positive peaks at ~1600 cm^{-1} observed at later times in polar solvents are better assigned to *trans*-enol DHHB (S_0) photoproducts, thereby accounting for the incomplete recovery of the GSB

features. A computational relaxed-geometry energy scan along the dihedral angle of the C(OH)–C–C=O portion of a DHHB molecule in the ground electronic state shows that the *trans*-enol is a metastable photoproduct because it must overcome a barrier to revert to the minimum energy structure (Figure S11). In contrast to DHHB, similar dynamics in photoexcited oxybenzone drive passage through an S_1 / S_0 conical intersection corresponding to a twisted S_1-keto structure, and further torsional dynamics on the S_0 potential energy surface lead to a minor *trans*-keto photoproduct.[15, 17] These differences between oxybenzone and DHHB relaxation pathways arise because in oxybenzone it is the S_1-keto form that has a twisted minimum energy structure, whereas in DHHB it is the S_1-enol form. The geometries of the conical intersections connecting these S_1 minima to the S_0 state influence the minor photoproduct isomers that form.

The absence of a band at 1600 cm^{-1} in TVA spectra for DHHB in CYCH is consistent with a greater propensity for ultrafast ESHT in the S_1 state. Decay from the resulting S_1-keto form is therefore proposed to be via an alternative pathway to the S_1 / S_0 conical intersection discussed above, which is argued to be located towards the twisted S_1-enol minimum energy structure. The GSB recovery approaches 98% in CYCH, and there is no obvious signature of *trans*-enol photoproduct formation. The remaining 2% is thus most likely to be a consequence of minor branching to triplet states of DHHB, and we suggest below that the outcome is population of the keto form of the T_1 state. In polar solvents, the GSB recoveries are about 95%, with the remaining 5% attributed in part to the *trans*-enol photoproducts seen by TVAS. The remainder is suggested to be a consequence of population of photoexcited triplet states, direct evidence for which comes from our TEAS measurements.

III.IV Triplet State Population and Quenching

The later time (>1000 ps) TEA spectra shown as insets in Figure 3 differ in their finer details in the various solvents. In MeOH, there is a long-lived absorption extending beyond 550 nm, whereas there is only weaker absorption beyond 600 nm for DHHB in CYCH. On the basis of electronic structure calculations (see Supporting Information), and quenching experiments described below, the longer-lived band seen at wavelengths beyond 550 nm is assigned to the T_1 state of DHHB. Data presented in Figure 7 show that the triplet-state ESA in methanol can be quenched by adding octocrylene, which is a common UVB absorber additive in sunscreen products. Further quenching tests were performed with *trans*-β-methylstyrene, which has a similar triplet-state energy to DHHB, and the TEA spectra of these mixtures are shown in Figure S12.[20, 46] Again, the longer-lived signal in the long wavelength region was quenched.

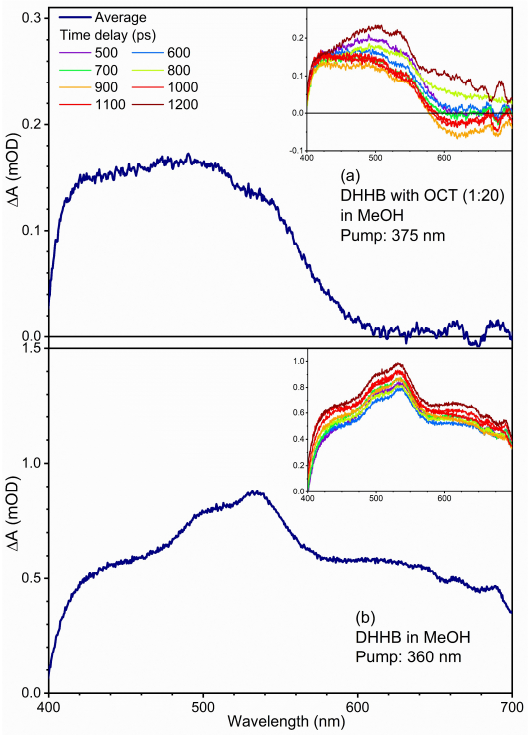

Figure 7. Plots of averaged late-time (500 – 1200 ps) TEA spectra of: (a) DHHB with added octocrylene (in 20-fold excess) and (b) DHHB in methanol. The insets display the individual spectra, and the colour key shows the time delays corresponding to each spectrum.

Just as for the singlet manifold of states, triplet spin state DHHB can exist in enol and keto forms. The computed UV-Vis absorptions of T_1 enol and T_1 keto DHHB are shown in Figure S13. Guided by these calculations, the long wavelength ESA feature observed at later times in methanol is assigned to the T_1 enol, because the calculated absorption bands of the T_1 keto form are located mainly in the 400 - 500 nm wavelength region. As Figure 7 shows, in the presence of octocrylene only a 400 - 500 nm ESA feature remains in the long-time spectra, which is attributed to the T_1-keto form of DHHB. Unlike the T_1-enol DHHB, this T_1-keto tautomer is not quenched by octocrylene because its triplet-state excitation energy is significantly smaller than that for the T_1 enol relative to their corresponding S_0 tautomers. The S_0-keto tautomer lies higher in energy than the S_0 enol, whereas the energy ordering is reversed in the T_1 state. Hence, the $T_1 - S_0$ energy gap in the keto form is insufficient to sensitize the octocrylene or *trans*-β-methylstyrene. The late time TEA spectra in CYCH (Figure S13) mainly show T_1 keto signals, consistent with the proposition that ESHT from S_1-enol to S_1-keto forms is more significant in CYCH. In DMSO, the T_1-enol absorption is weaker than in the other polar solvents, and the late time spectra look similar to those

obtained in CYCH. These observations are taken as further evidence that that the more viscous solvent environment in DMSO slows down C-C twisting in the S_1 enol and instead promotes ESHT.

Transient absorption spectra of DHHB in ethanol, obtained at time delays of 0.3 - 1.2 μs by Shamoto et al. show a broad ESA signature peaking near 400 nm and extending up to ~500 nm that resembles the ESA band we assign to the T_1-keto tautomer.[20] Our mechanistic arguments suggest the T_1-enol tautomer should be preferentially formed in protic solvents (e.g. MeOH or ethanol) which suppress the ESHT, but in the T_1 state, the keto form is computed to lie lower in energy than the enol form. Hence, it is possible that the T_1 enol undergoes hydrogen transfer to the T_1 keto with a nanosecond to microsecond time constant that is outside the time window of our ultrafast spectroscopy experiments but accessible to the measurements of Shamoto et al. In their experiments using DHHB in 3-methylpentane, this T_1 keto ESA was not observed, which suggests either that the T_1 keto lifetime is < 0.3 μs, or that S_1-state ESHT (favoured in non-polar solvents) hinders the intersystem crossing (ISC) from singlet to triplet states. The combined evidence from this prior and our current work points to the ISC occurring from the vicinity of the twisted S_1-enol geometry, in competition with internal conversion to S_0 via a conical intersection. However, our later time TEA spectra of DHHB in CYCH do not show the ESA features assigned to the T_1-enol form, although bands are evident which could correspond to the T_1-keto form (on the basis of the aforementioned calculations). Thus, there may also be an accessible ISC pathway from the S_1-keto to the T_1-keto forms.

IV. Conclusion

Ultrafast transient absorption spectra of the sunscreen compound DHHB, photoexcited at wavelengths around 360 nm and 345 nm, differ significantly in polar and non-polar solvents. In the non-polar cyclohexane, ESHT happens in <200 fs from the Franck-Condon region of the S_1 state, converting the S_1-enol to the S_1-keto form, and is the main dynamical pathway. Evidence is presented from TEA spectra that a small fraction of the S_1-keto intermediate subsequently populates the T_1 state in its keto form via intersystem crossing. However, TVA spectra show that >98% of the photoexcited DHHB relaxes back to the ground state with an exponential time constant of ~12ps. In three chosen polar solvents, methanol, acetonitrile and DMSO, disruption of the intramolecular hydrogen bond in DHHB inhibits ESHT from the initially excited S_1-state enol. Therefore, a greater proportion of the photoexcited DHHB retains its S_1-enol character and relaxes by C-C bond torsion that quenches stimulated emission bands observed by TEAS with a solvent-dependent time constant of 300 – 800 fs. A small fraction (≤5%) of the twisted S_1-enol intermediates undergoes intersystem crossing to the T_1 enol, which is observed by TEAS at later time delays. This T_1 enol population can be quenched by adding octocrylene (a UVB absorber), showing that sunscreen

formulations containing both DHHB and octocrylene can influence the sun protection efficiency. The octocrylene should inhibit build-up of undesirable DHHB (T_1) photoproducts, but could itself be sensitized to an excited triplet state in the process. A competing photoproduct, the *trans*-enol isomer of DHHB, is formed via a conical intersection between the S_1 and S_0 states, and is directly observed in low yield by TVAS of photoexcited DHHB in polar solvents. The remaining 95% of photoexcited DHHB relaxes back to the minimum energy structure on the S_0 ground-electronic state with a time constant of ~15 ps that is associated with a combination of S_1-state decay and vibrational cooling of internally excited S_0 molecules. Although DHHB and oxybenzone are structurally similar, differences in their S_1 PESs for keto and enol forms substantially change the relaxation pathways that are essential for good sunscreen performance.

Data Availability: Data are available at the University of Bristol data repository, data.bris [DOI to be added upon acceptance of the manuscript].

Supporting Information. Computed structures and tautomerization pathways for S_0 and S_1 state DHHB molecules. Steady-state UV-Vis, FTIR, and fluorescence spectra of DHHB in the four solvents. Computed electronic excitations from the S_0 and S_1 states of DHHB. Examples of decomposition of TEA spectra of photoexcited DHHB in methanol and cyclohexane solutions. Late-time TVA spectra of DHHB. Experimental and computational evidence for the trans-enol photoproduct. TEA spectra for DHHB solutions with added *trans*-beta-methylstyrene. Computational assignment of experimentally observed DHHB T_1 keto and enol excited state absorption bands.

Acknowledgements: The ultrafast laser laboratory at the University of Bristol was established with funding from ERC Advanced Grant 290966 CAPRI. BASF generously provided a sample of Uvinul A Plus for this research. RKV was supported by a SERB-Royal Society Newton International Fellowship (NF160517), and MS gratefully acknowledges support through the Marie-Skłodowska Curie fellowship MARCUS 793799.

References

1. Sage, E.; Girard, P. M.; Francesconi, S., Unravelling UVA-induced mutagenesis. *Photochem. Photobiol. Sci.* **2012,** *11*, 74-80.
2. Attard, N. R.; Karran, P., UVA photosensitization of thiopurines and skin cancer in organ transplant recipients. *Photochem. Photobiol. Sci.* **2012,** *11*, 62-68.

3. Pfeifer, G. P.; Besaratinia, A., UV wavelength-dependent DNA damage and human non-melanoma and melanoma skin cancer. *Photochem. Photobiol. Sci.* **2012,** *11*, 90-97.
4. Sample, A.; Zhao, B. Z.; Qiang, L.; He, Y. Y., Adaptor protein p62 promotes skin tumor growth and metastasis and is induced by UVA radiation. *J. Biol. Chem.* **2017,** *292*, 14786-14795.
5. Sutherland, J. C.; Griffin, K. P., Absorption-spectrum of DNA for wavelengths greater than 300-nm. *Radiat. Res.* **1981,** *86*, 399-410.
6. Wondrak, G. T.; Roberts, M. J.; Cervantes-Laurean, D.; Jacobson, M. K.; Jacobson, E. L., Proteins of the extracellular matrix are sensitizers of photo-oxidative stress in human skin cells. *J. Invest. Dermatol.* **2003,** *121*, 578-586.
7. Bruge, F.; Tiano, L.; Astolfi, P.; Emanuelli, M.; Damiani, E., Prevention of UVA-induced oxidative damage in human fermal fibroblasts by new UV filters, assessed using a novel in vitro experimental system. *PLoS One* **2014,** *9*, 11.
8. Osterwalder, U.; Sohn, M.; Herzog, B., Global state of sunscreens. *Photodermatol. Photo.* **2014,** *30*, 62-80.
9. Shaath, N. A., Ultraviolet filters. *Photochem. Photobiol. Sci.* **2010,** *9*, 464-469.
10. Kawakami, C. M.; Maximo, L. N. C.; Fontanezi, B. B.; da Silva, R. S.; Gaspar, L. R., Diethylamino hydroxybenzoyl hexyl benzoate (DHHB) as additive to the UV filter avobenzone in cosmetic sunscreen formulations - Evaluation of the photochemical behavior and photostabilizing effect. *Eur. J. Pharm. Sci.* **2017,** *99*, 299-309.
11. Lhiaubet-Vallet, V.; Marin, M.; Jimenez, O.; Gorchs, O.; Trullas, C.; Miranda, M. A., Filter-filter interactions. Photostabilization, triplet quenching and reactivity with singlet oxygen. *Photochem. Photobiol. Sci.* **2010,** *9*, 552-558.
12. Cho, Y. T.; Su, H.; Huang, I. C.; Lai, C. Y.; Tsai, Y. D., Rapid characterization of organic UV filters and their photoproducts in sunscreens by thermal desorption electrospray ionization mass spectrometry for the photostability study. *Anal. Methods* **2019,** *11*, 6013-6022.
13. Ouchene, L.; Litvinov, I. V.; Netchiporouk, E., Hawaii and other jurisdictions ban oxybenzone or octinoxate sunscreens based on the confirmed adverse environmental effects of sunscreen ingredients on aquatic environments. *J. Cutan. Med. Surg.* **2019,** *23*, 648-649.
14. Downs, C. A.; Kramarsky-Winter, E.; Segal, R.; Fauth, J.; Knutson, S.; Bronstein, O.; Ciner, F. R.; Jeger, R.; Lichtenfeld, Y.; Woodley, C. M.; Pennington, P.; Cadenas, K.; Kushmaro, A.; Loya, Y., Toxicopathological effects of the sunscreen UV filter, oxybenzone (benzophenone-3), on coral planulae and cultured primary cells and its environmental contamination in Hawaii and the US Virgin Islands. *Arch. Environ. Contam. Toxicol.* **2016,** *70*, 265-288.
15. Baker, L. A.; Horbury, M. D.; Greenough, S. E.; Coulter, P. M.; Karsili, T. N.; Roberts, G. M.; Orr-Ewing, A. J.; Ashfold, M. N.; Stavros, V. G., Probing the Ultrafast Energy Dissipation Mechanism of the Sunscreen Oxybenzone after UVA Irradiation. *J. Phys. Chem. Lett.* **2015,** *6*, 1363-8.
16. Li, C. X.; Guo, W. W.; Xie, B. B.; Cui, G., Photodynamics of oxybenzone sunscreen: Nonadiabatic dynamics simulations. *J. Chem. Phys.* **2016,** *145*, 074308.
17. Karsili, T. N. V.; Marchetti, B.; Ashfold, M. N. R.; Domcke, W., Ab Initio study of potential ultrafast internal conversion routes in oxybenzone, caffeic acid, and ferulic acid: implications for sunscreens. *J. Phys. Chem. A* **2014,** *118*, 11999-12010.
18. Ignasiak, M. T.; Houée-Levin, C.; Kciuk, G.; Marciniak, B.; Pedzinski, T., A Reevaluation of the Photolytic Properties of 2-Hydroxybenzophenone-Based UV Sunscreens: Are Chemical Sunscreens Inoffensive? *ChemPhysChem* **2015,** *16*, 628-633.
19. Hou, S. Y.; Hetherington, W. M.; Korenowski, G. M.; Eisenthal, K. B., Intra-molecular proton-transfer and energy relaxation in ortho-hydroxybenzophenone. *Chem. Phys. Lett.* **1979,** *68*, 282-284.
20. Shamoto, Y.; Yagi, M.; Oguchi-Fujiyama, N.; Miyazawa, K.; Kikuchi, A., Photophysical properties of hexyl diethylaminohydroxybenzoylbenzoate (Uvinul A Plus), a UV-A absorber. *Photochem. Photobiol. Sci.* **2017,** *16*, 1449-1457.
21. Beeby, A.; Jones, A. E., The photophysical properties of menthyl anthranilate: A UV-A sunscreen. *Photochem. Photobiol.* **2000,** *72*, 10-15.
22. Kikuchi, A.; Shibata, K.; Kumasaka, R.; Yagi, M., Excited states of menthyl anthranilate: a UV-A absorber. *Photochem. Photobiol. Sci.* **2013,** *12*, 246-253.
23. Kikuchi, A.; Oguchi-Fujiyama, N.; Miyazawa, K.; Yagi, M., Triplet-triplet energy transfer from a UV-A absorber butylmethoxydibenzoylmethane to UV-B absorbers. *Photochem. Photobiol.* **2014,** *90*, 511-516.
24. Matsumoto, S.; Kumasaka, R.; Yagi, M.; Kikuchi, A., Triplet-triplet energy transfer between UV absorbers in solutions at room temperature. *J. Photochem. Photobiol. A* **2017,** *346*, 396-400.

25. Kikuchi, A.; Nakabai, Y.; Oguchi-Fujiyama, N.; Miyazawa, K.; Yagi, M., Energy-donor phosphorescence quenching study of triplet-triplet energy transfer between UV absorbers. *J. Lumines.* **2015,** *166*, 203-208.
26. Roberts, G. M.; Marroux, H. J. B.; Grubb, M. P.; Ashfold, M. N. R.; Orr-Ewing, A. J., On the participation of photoinduced N-H bond fission in aqueous adenine at 266 and 220 nm: a combined ultrafast transient electronic and vibrational absorption spectroscopy study. *J. Phys. Chem. A* **2014,** *118*, 11211-11225.
27. Rottger, K.; Marroux, H. J. B.; Chemin, A. F. M.; Elsdon, E.; Oliver, T. A. A.; Street, S. T. G.; Henderson, A. S.; Galan, M. C.; Orr-Ewing, A. J.; Roberts, G. M., Is UV-induced electron-driven proton transfer active in a chemically modified A - T DNA base pair? *J. Phys. Chem. B* **2017,** *121*, 4448-4455.
28. Grubb, M. P.; Orr-Ewing, A. J.; Ashfold, M. N. R., KOALA: A program for the processing and decomposition of transient spectra. *Rev. Sci. Instrum.* **2014,** *85*, 064104.
29. Frisch, M. J.; Trucks, G. W.; Schlegel, H. B.; Scuseria, G. E.; Robb, M. A.; Cheeseman, J. R.; Scalmani, G.; Barone, V.; Mennucci, B.; Petersson, G. A.; et al., Gaussian 09, Revision D.01, Gaussian Inc., Wallingford CT,. **2013**.
30. Barone, V.; Cossi, M., Quantum calculation of molecular energies and energy gradients in solution by a conductor solvent model. *J. Phys. Chem. A* **1998,** *102*, 1995-2001.
31. Cossi, M.; Rega, N.; Scalmani, G.; Barone, V., Energies, structures, and electronic properties of molecules in solution with the C-PCM solvation model. *J. Comput. Chem.* **2003,** *24*, 669-681.
32. Frisch, M. J.; Pople, J. A.; Binkley, J. S., Self-consistent molecular orbital methods 25. Supplementary functions for Gaussian basis sets. *J. Chem. Phys.* **1984,** *80*, 3265-3269.
33. Hehre, W. J.; Ditchfield, R.; Pople, J. A., Self—Consistent Molecular Orbital Methods. XII. Further Extensions of Gaussian—Type Basis Sets for Use in Molecular Orbital Studies of Organic Molecules. *J. Chem. Phys.* **1972,** *56*, 2257.
34. Parr, R. G.; Yang, W. T., Density-Functional Theory of the Electronic Structure of Molecules. *Annu. Rev. Phys. Chem.* **1995,** *46*, 701-728.
35. Becke, A. D., Density-functional thermochemistry. III. The role of exact exchange. *J. Chem. Phys.* **1993,** *98*, 5648-5652.
36. Lee, C. T.; Yang, W. T.; Parr, R. G., Development of the Colle-Salvetti correlation-energy formula into a functional of the electron density. *Phys. Rev. B* **1988,** *37*, 785-789.
37. Runge, E.; Gross, E. K. U., Density-functional theory for time-dependent systems. *Phys. Rev. Lett.* **1984,** *52*, 997-1000.
38. Urahata, S.; Canuto, S., Monte Carlo-quantum mechanics study of the UV-visible spectrum of benzophenone in water. *Int. J. Quantum Chem.* **2000,** *80*, 1062-1067.
39. Kumar, V. R.; Rajkumar, N.; Umapathy, S., Solvatochromism of 9,10-phenanthrenequinone: An electronic and resonance Raman spectroscopic study. *J. Chem. Phys.* **2015,** *142*, 12.
40. Kumar, V. R.; Verma, C.; Umapathy, S., Molecular dynamics and simulations study on the vibrational and electronic solvatochromism of benzophenone. *J. Chem. Phys.* **2016,** *144*, 12.
41. Marcus, Y., The properties of organic liquids that are relevant to their use as solvating solvents. *Chem. Soc. Rev.* **1993,** *22*, 409-416.
42. Herek, J. L.; Pedersen, S.; Banares, L.; Zewail, A. H., Femtosecond real-time probing of reactions. IX. Hydrogen-atom transfer. *J. Chem. Phys.* **1992,** *97*, 9046-9061.
43. Horke, D. A.; Watts, H. M.; Smith, A. D.; Jager, E.; Springate, E.; Alexander, O.; Cacho, C.; Chapman, R. T.; Minns, R. S., Hydrogen bonds in excited state proton transfer. *Phys. Rev. Lett.* **2016,** *117*, 5.
44. Watwiangkham, A.; Roongcharoen, T.; Kungwan, N., Effect of nitrogen substitution and pi-conjugation on photophysical properties and excited state intramolecular proton transfer reactions of methyl salicylate derivatives: Theoretical investigation. *J. Photochem. Photobiol. A* **2020,** *389*, 11.
45. Holt, E. L.; Krokidi, K. M.; Turner, M. A. P.; Mishra, P.; Zwier, T. S.; Rodrigues, N. D. N.; Stavros, V. G., Insights into the photoprotection mechanism of the UV filter homosalate. *Phys. Chem. Chem. Phys.* **2020,** *22*, 15509-15519.
46. Crosby, P. M.; Dyke, J. M.; Metcalfe, J.; Rest, A. J.; Salisbury, K.; Sodeau, J. R., The Triplet State of Styrenes. *J. Chem. Soc.-Perkin Trans. 2* **1977**, 182-185.

ToC Graphic

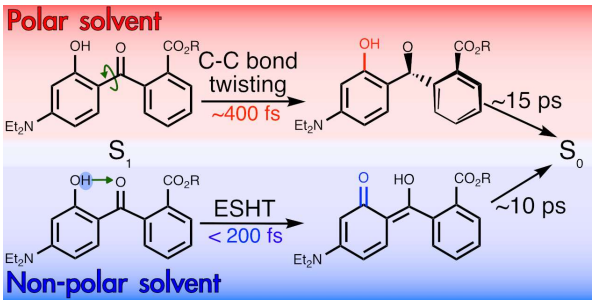
Polar solvent
OH
O
CO2R
Et2N
C-C bond
twisting
~400 fs
OH
O
CO2R
Et2N
~15 ps
S1
S0
OH
O
CO2R
Et2N
ESHT
< 200 fs
O
HO
CO2R
Et2N
~10 ps
Non-polar solvent